Deep Learning Based Uplink Precoding for High Speed Train Communications in FD-RAN

Zeyu Sun*, Jiwei Zhao†, Yunting Xu*, Jiacheng Chen‡, Haibo Zhou*, Lian Zhao§
*School of Electronic Science and Engineering, Nanjing University.
{zeyusun, yuntingxu}@smail.nju.edu.cn, haibozhou@nju.edu.cn
†Information Science and Electronic Engineering, Zhejiang University. jackokie@zju.edu.cn
‡Department of Strategic and Advanced Interdisciplinary Research, Peng Cheng Laboratory. chenjch02@pcl.ac.cn
§Department of Electrical, Computer, Biomedical Engineering, Toronto Metropolitian University. l5zhao@torontomu.ca

2024 IEEE 99th Vehicular Technology Conference (VTC2024-Spring) | 979-8-3503-8741-4/24/$31.00 ©2024 IEEE | DOI: 10.1109/VTC2024-SPRING62846.2024.10683311

***Abstract*—High speed train (HST) communications with multi-user multiple-input multiple-output (MU-MIMO) techniques have shown great potential in system performance improvements. However, the challenges caused by higher pilot overhead and the belated channel state information (CSI) feedback in such high mobility scenarios still need to be further addressed. To this end, fully-decoupled radio access network (FD-RAN) with novel location-based feedback-free transmission scheme and cooperative transmission/reception in separated downlink/uplink networks is regarded as a promising solution. In this paper, we study the uplink precoding design in FD-RAN for HST communications. To capture the inherent relation between location and precoding, the line-of-sight (LoS) channel is derived from location and then fed into a proposed precoding design neural network (PDNN) which learns to jointly optimize the precoding scheme for all the multi-antenna mobile relays (MRs) in uplink MU-MIMO. We adopt a custom loss function to optimize the spectrum efficiency (SE). Moreover, a joint signal reception method is given, also based solely on the LoS channel derived from location, so as to avoid frequent pilot transmission. Simulation results show the advantages of FD-RAN against other architectures and demonstrate that our proposed PDNN achieves better performance than traditional precoding scheme in high mobility scenarios.**

***Index Terms*—High speed train communications, FD-RAN, MU-MIMO, deep learning, precoding design**

I. Introduction

With the booming development of railway system, high-speed train (HST) communications have received significant attention [1]. In the fifth generation mobile networks (5G), profound performance improvement has been realized through massive multi-input multi-output (mMIMO) with joint precoding design, which can exploit the diversity and multiplexing gains. However, high mobility will deteriorate the channel in many aspects, such as Doppler frequency offset (DFO), shorter coherence time and phase noise, leading to severe performance decline in HST systems [2]. Additionally, there will be more frequent handover between base stations (BSs). Traditional solutions such as long term evolution for railway (LTE-R) employ more frequent pilot transmission and channel state information (CSI) feedback, consuming a considerable amount of time-frequency resources [3]. Furthermore, due to feedback delay, it is difficult to acquire the accurate CSI [4].

The sixth-generation (6G) mobile communication networks are expected to provide more flexible resource allocation and enhance users' experiences. Specifically, an original architecture named fully-decoupled radio access networks (FD-RAN) [5] was proposed, which decouples BSs into uplink base stations (UBSs), downlink base stations (DBSs) and control BSs. FD-RAN has several advantages for HST communications. On the one hand, with all the control plane signalling taken over by the control BSs, which cover a much larger area like cloud RAN, handover overheads can be largely reduced. On the other hand, FD-RAN adopts geolocation-based feedback-free transmission scheme [6] for MIMO. Through this scheme, not only the negative effects of channel variation and resource overheads can be mitigated, but also feedback delay can be avoided through location prediction, which is trivial for HST.

Although the feedback-free transmission based on the FD-RAN architecture is trivial for HST communications, it is still challenging to determine appropriate MIMO precoding only from location information [7]. Furthermore, considering the multiple mobile relays (MRs) equipped on the HST, multi-user MIMO (MU-MIMO) scenario should be utilized, thus joint precoding design is required. Besides, to save more pilot resources, signal reception at the UBSs cannot utilize the realtime channel estimated from pilot either.

In order to address the above challenges, this paper develops a precoding design neural network (PDNN) to learn to maximize the overall spectrum efficiency (SE) by jointly optimizing the precoding for all the transmitters. Instead of taking location as input directly, the line-of-sight (LoS) channel is first estimated based on location and then fed into PDNN, such that the strong correlation between channel and location can be utilized in HST communications scenario. The same estimated LoS channel is also used at UBSs for signal detection, thus traditional pilot are not required. The contributions of this paper are summarized as follows:

- An uplink feedback-free MU-MIMO transmission scheme for HST communications based on the FD-RAN architecture is proposed so as to reduce the overheads

This work was supported in part by the National Natural Science Foundation Original Exploration Project of China under Grant 62250004, the Natural Science Foundation of China (NSFC) under Grant 62271244, Innovation and Entrepreneurship of Jiangsu Province High-level Talent Program, Summit of the Six Top Talents Program of Jiangsu Province, The Major Key Project of PCL, and The Basic and Frontier Research Project of PCL.

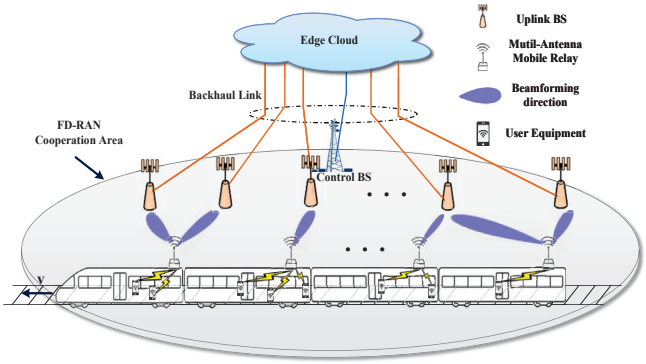

Fig. 1: HST uplink communication with FD-RAN system.

of pilot transmission and overcome feedback delay. Only the LoS channel derived directly from the train's location is required for both joint precoding design and signal reception at the UBSs.

- To achieve the real-time precoding design, we adopt a complex valued neural network that can converge to the optimal within few epochs. The derived LoS channel is fed into the neural network, and aims at maximizing the SE (i.e., minimizing the loss function) by learning the precoding for all MRs jointly.
- We perform simulations and analysis for our proposed scheme. The results demonstrate that our method has advantages against other RAN architectures and achieves better performance than traditional precoding scheme in HST communications.

The remainder of this paper is structured as follows: Section II presents the system model and outlines the problem formulation of the feedback-free transmission approach in HST communications scenario. Then, in Section III, the neural network architecture and training procedure is explained. Next, the simulation results and comparisons are shown in Section IV. Finally, the conclusions and future directions are drawn in Section V.

II. System Model and Problem Formulation

As illustrated in Fig. 1, we consider a MU-MIMO enabled HST communications system in FD-RAN, which consists of K MRs with N_V antennas at speed v, and L UBSs with N_B antennas. The passengers' user equipments (UEs) communicate with the UBSs through the MRs on the top of trains. The wide coverage control BS is the controller and coordinator for all UBSs and MRs located in the FD-RAN. All BSs connect to the edge cloud via backhaul links. We consider joint signal reception such that all L UBSs serve all K MRs at the same time. Additionally, we adopt the large-scale fading decoding (LSFD) receiver which can achieve doubled gain than traditional receivers like matched filter (MF) in cell-free system with similar uplink topology [8].

A. Propagation Model

The typical channel for HST communications includes tunnels and viaducts. Particularly, 86.5% of the railways are viaducts in Beijing-Shanghai HST [8]. Because of little reflection and scattering, there are few multi-path propagation in HST. Thus the LoS channel is widely assumed in HST communications studies [9]. However, in order to characterize the realistic channel comprising NLoS paths [10], we adopt the Rician fading model which utilizes a R-factor to describe the relative strength of LoS and NLoS components.

Supposed that UBSs are deployed along the railway track and both K MRs and L UBSs are uniformly linear distributed [9]. The vertical height of UBSs are denoted as d^{ve} and d_{kl} represents the distance between MR k and UBS l. Then, the sine value of the angle of departure (AoD) θ_{kl} between UBS l and MR k is formulated as

$$\sin\theta_{kl} = \frac{d^{\text{ve}}}{d_{kl}}. \tag{1}$$

Considering the significant LoS component in HST communications scenario, we model the large-scale fading between UBS l and MR k as $\beta_{kl} = (d_{kl})^{-\alpha/2}$, where $\alpha \in [2:6]$. Then, the MIMO channel matrix attached to the LoS link can be given by (2) next page, where d_B and d_V represent the antenna spacing parameter (in fractions of wavelength λ) at UBSs and MRs, respectively. The matrix component is the product of the specular array responses at UBSs and moving MRs. Additionally, the DFO resulted from the high speed is also taken into account, given by $\frac{fc}{v}\cos\theta$, where f and θ are the carrier frequency and AoD [9]. The velocity of light is denoted as c.

Besides LoS component, the channel is also affected by the multi-path fading [11] denoted as $\mathbf{H}^{(\text{multi}-\text{path})}$. The m-th path between MR k and UBS l is represented as $\mathbf{H}^{(\text{multi}-\text{path})}_{kl,m}$, which can be formulated similar to (2). The difference is the large-scale fading coefficient and random AoD $\theta_{kl,m}$.

Based on the analysis above, the channel with M multi-path between the moving MR k and UBS l can be modeled by (3), where $\exp\left(j2\pi\frac{fc}{v}\cos\theta_{kl}\right)$ characterizes the phase change caused by DFO. The AoD of m-th path between MR k and UBS l, $\theta_{kl,m}$ follows a uniform distribution over the interval from 0 to π. $R \geq 0$ is the Rician factor. When $R \to \infty$, the channel is considered as a pure LoS channel without any multi-path components and $R = 0$ represents that the channel degenerates into a Rayleigh fading channel.

B. Feedback-free Uplink Transmission

1) Location-channel mapping: Due to the physical decoupling of uplink and downlink BSs in FD-RAN system and the high mobility of HST, it is difficult to acquire accurate and real-time CSI by traditional pilot estimation. In practical systems, the location of UBSs and MRs are able to be obtained in advance because of the steadiness of the train track and the train operation schedule. Additionally, the velocity of HST v would not change drastically and can be obtained by the train

$$\mathbf{H}_{kl}^{(\mathrm{LoS})} = \beta_{kl} \begin{pmatrix} 1 & \cdots & \exp\left[-j2\pi \frac{d_V}{\lambda}\left(N_V-1\right)\cos\theta_{kl}\right] \\ \vdots & \ddots & \vdots \\ \exp\left[j2\pi \frac{d_B}{\lambda}\left(N_B-1\right)\cos\theta_{kl}\right] & \cdots & \exp\left\{j2\pi\cos\theta_{kl}\left[\frac{d_B}{\lambda}\left(N_B-1\right)-\frac{d_V}{\lambda}\left(N_V-1\right)\right]\right\} \end{pmatrix}. \tag{2}$$

$$\mathbf{H}_{kl} = \frac{1}{\sqrt{R+1}}\left[\sqrt{R}\exp\left(j2\pi\frac{fc}{v}\cos\theta_{kl}\right)\mathbf{H}_{kl}^{(\mathrm{LoS})} + \sum_{m=1}^{M}\sqrt{\frac{1}{M}}\exp\left(j2\pi\frac{fc}{v}\cos\theta_{kl,m}\right)\mathbf{H}_{kl,m}^{(\mathrm{multi-path})}\right]. \tag{3}$$

control system. Therefore, $\mathbf{H}_{kl}^{(\mathrm{LoS})}$ can be determined by (2). In order to achieve feedback-free transmission, we take the pure LoS channel component $\hat{\mathbf{H}}_{kl}$ between MR k and UBS l derived from (4) as the estimation, which can be directly obtained from geolocation and the velocity of HST,

$$\hat{\mathbf{H}}_{kl} = \exp\left(j2\pi\frac{fc}{v}\cos\theta_{kl}\right)\mathbf{H}_{kl}^{(\mathrm{LoS})}. \tag{4}$$

Note that $\hat{\mathbf{H}}_{kl}$ is directly modeled by mathematical formula, and the estimation is therefore less precise than traditional methods that utilize pilot. The estimation error $\tilde{\mathbf{H}}_{kl}$ is given by

$$\begin{aligned}\tilde{\mathbf{H}}_{kl} &= \mathbf{H}_{kl} - \hat{\mathbf{H}}_{kl} \\ &= \frac{1}{\sqrt{\sigma+1}}\sum_{m=1}^{M}\sqrt{\frac{1}{M}}\exp\left(j2\pi\frac{fc}{v}\cos\theta_{kl,m}\right)\mathbf{H}_{kl,m}^{(\mathrm{multi-path})}\end{aligned} \tag{5}$$

which is contingent upon the intensity of multi-path components and exhibits an inverse relationship with the Rician factor R. In other words, the location-channel mapping is more accurate when the LoS component becomes more dominant.

2) Data transmission: The transmitted signal $\mathbf{s}_k$ from MR k can be constructed as $\mathbf{s}_k = \mathbf{P}_k x_k$, where x_k is the data symbol from MR k, satisfying that $\mathbb{E}\{x_k\} = 0$ and $\mathbb{E}\{x_k^2\} = 1$. $\mathbf{P}_k \in \mathbb{C}^{N_V \times 1}$ is the precoding vector during the data transmission phase satisfying $tr(\mathbf{P}_k\mathbf{P}_k^{\mathrm{H}}) \le p_k$, which represents the power constraint of MR k where p_k denoting the maximum transmitted power.

The received signal $\mathbf{y}_l$ at UBS l is

$$\mathbf{y}_l = \sum_{k=1}^{K}\mathbf{H}_{kl}\mathbf{P}_k x_k + \mathbf{n}_l = \sum_{k=1}^{K}\mathbf{H}_{kl}\mathbf{s}_k + \mathbf{n}_l, \tag{6}$$

where $\mathbf{n}_l \sim (0, \sigma^2\mathbf{I}_{N_B})$ is the independent receiver noise and σ^2 represents the noise power.

3) Signal detection: Previous work [12] has investigated LSFD based two-tier signal combination approach for FD-RAN uplink transmission with multi-antenna UBSs and single-antenna transmitter UEs. We further investigate this approach with multi-antenna MRs in FD-RAN uplink transmission.

The two-tier decoding scheme includes the localized signal processing at UBSs and centralized signal combination at the edge cloud. Denoting $\mathbf{W}_{kl} \in \mathbb{C}^{N_B \times 1}$ as the combining vector calculated by UBS l for MR k, the local estimate $\tilde{x}_{kl}$ at UBS l is

$$\begin{aligned}\tilde{x}_{kl} &= \mathbf{W}_{kl}^{\mathrm{H}}\mathbf{y}_l \\ &= \mathbf{W}_{kl}^{\mathrm{H}}\mathbf{H}_{kl}\mathbf{P}_k x_k + \sum_{n=1,n\neq k}^{K}\mathbf{W}_{kl}^{\mathrm{H}}\mathbf{H}_{nl}\mathbf{P}_n x_n + \mathbf{W}_{kl}^{\mathrm{H}}\mathbf{n}_l.\end{aligned} \tag{7}$$

We leverage the Local MMSE (L-MMSE) combining that minimizes the mean-squared error [13] as

$$\begin{aligned}\mathbf{W}_{kl} &= \arg\min_{\mathbf{W}_{kl}}\mathbb{E}\left\{\left|x_k - \mathbf{W}_{kl}^{\mathrm{H}}\mathbf{y}_l\right|^2 | \hat{\mathbf{H}}_{kl}\right\} \\ &= \left(\sum_{n=1}^{K}\left(\hat{\mathbf{H}}_{nl}\overline{\mathbf{P}}_n\hat{\mathbf{H}}_{nl}^{\mathrm{H}}\right) + \mathbf{C}_{nl} + \sigma^2\mathbf{I}_{N_B}\right)^{-1}\hat{\mathbf{H}}_{kl}\mathbf{P}_k,\end{aligned} \tag{8}$$

where $\mathbf{C}_{nl} \triangleq \mathbb{E}\left\{\tilde{\mathbf{H}}_{nl}\overline{\mathbf{P}}_n\tilde{\mathbf{H}}_{nl}^{\mathrm{H}}\right\}$ represents the error term and $\overline{\mathbf{P}}_n \triangleq \mathbf{P}_n\mathbf{P}_n^{\mathrm{H}}$.

The second-tier combination LSFD [12] is implemented and a centralized combination at the edge cloud is deployed to decode all the local estimation signal $\tilde{x}_{kl}$ for any MR k. We define the effective channel from MR k to all UBSs as

$$\mathbf{G}_{kn} \triangleq \left[\mathbf{W}_{k1}^{\mathrm{H}}\mathbf{H}_{n1}, \cdots, \mathbf{W}_{kL}^{\mathrm{H}}\mathbf{H}_{nL}\right]^{\mathrm{T}}. \tag{9}$$

At the edge cloud, all the local estimates are weighted by the centralized combination coefficient a_{kl}, which represents the complex second-tier combination coefficient for UBS l and MR k. Then the centralized processing signal for MR k can be given as (10).

We define $\mathbf{A}_k \triangleq [a_{k1}, \cdots, a_{kL}]^{\mathrm{T}}$ and apply the classical use-and-then-forget (UatF) bound [13] to compute the achievable signal to interference plus noise ratio (SINR) given in (11), where $\mathbf{N}_k \triangleq \mathrm{diag}\left(\mathbb{E}\{\mathbf{W}_{k1}^{\mathrm{H}}\mathbf{W}_{k1}\}, \cdots, \mathbb{E}\{\mathbf{W}_{kL}^{\mathrm{H}}\mathbf{W}_{kL}\}\right)$.

The complex second-tier combination coefficient matrix $\mathbf{A}_k$ can be optimized by the edge cloud to achieve the SE (12) for MR k as the following equation [14],

$$\mathbf{A}_k = \left(\sum_{n=1}^{K}\left\{\mathbf{G}_{kn}\overline{\mathbf{P}}_n\mathbf{G}_{kn}^{\mathrm{H}}\right\} + \sigma^2\mathbf{N}_k\right)^{-1}\left\{\mathbf{G}_{kk}\right\}\mathbf{P}_k. \tag{13}$$

$$\begin{aligned}\hat{x}_k &= \sum_{l=1}^{L} a_{kl}\tilde{x}_{kl} = \sum_{l=1}^{L} a_{kl}\mathbf{W}_{kl}^{\mathrm{H}}\mathbf{H}_{kl}\mathbf{P}_k x_k + \sum_{l=1}^{L}\sum_{n=1,n\neq k}^{K} a_{kl}\mathbf{W}_{kl}^{\mathrm{H}}\mathbf{H}_{nl}\mathbf{P}_n x_n + a_{kl}\mathbf{W}_{kl}^{\mathrm{H}}\mathbf{n}_l \\ &= \sum_{l=1}^{L} a_{kl}\mathbf{G}_{kk}\mathbf{P}_k x_k + \sum_{l=1}^{L}\sum_{n=1,n\neq k}^{K} a_{kl}\mathbf{G}_{kn}\mathbf{P}_n x_n + \hat{\mathbf{n}}_k.\end{aligned} \tag{10}$$

$$\mathrm{SINR}_k = \mathbf{P}_k^{\mathrm{H}}\mathbb{E}\left\{\mathbf{G}_{kk}^{\mathrm{H}}\right\}\mathbf{A}_k\left(\sum_{n=1}^{K}\mathbf{A}_k^{\mathrm{H}}\mathbb{E}\left\{\mathbf{G}_{kn}\overline{\mathbf{P}}_n\mathbf{G}_{kn}^{\mathrm{H}}\right\}\mathbf{A}_k - \mathbf{A}_k^{\mathrm{H}}\mathbb{E}\left\{\mathbf{G}_{kk}\right\}\overline{\mathbf{P}}_k\mathbb{E}\left\{\mathbf{G}_{kn}^{\mathrm{H}}\right\}\mathbf{A}_k + \sigma^2\mathbf{A}_k^{\mathrm{H}}\mathbf{N}_k\mathbf{A}_k\right)^{-1}\mathbf{A}_k^{\mathrm{H}}\mathbb{E}\left\{\mathbf{G}_{kk}\right\}\mathbf{P}_k. \tag{11}$$

$$\mathrm{SE}_k = \left(1-\frac{\tau_p}{\tau_c}\right)\log_2\left|1+\mathbf{P}_k^{\mathrm{H}}\mathbb{E}\left\{\mathbf{G}_{kk}^{\mathrm{H}}\right\}\left(\sum_{n=1}^{K}\mathbb{E}\left\{\mathbf{G}_{kn}\overline{\mathbf{P}}_n\mathbf{G}_{kn}^{\mathrm{H}}\right\} - \mathbb{E}\left\{\mathbf{G}_{kk}\right\}\overline{\mathbf{P}}_k\mathbb{E}\left\{\mathbf{G}_{kn}^{\mathrm{H}}\right\} + \sigma^2\mathbf{N}_k\right)^{-1}\mathbb{E}\left\{\mathbf{G}_{kk}\right\}\mathbf{P}_k\right|. \tag{12}$$

C. Problem Formulation

In MU-MIMO scenarios, studying the precoding design is vital to leverage the transmission gain of multi-antenna and minimize the interference. In this paper, the sum SE of all MRs is choosen as the optimization objective and the optimization problem is formulated as the joint design of precoding for all MRs to maximize sum SE. Then denoting all the precoding of MRs as $\mathbf{P} \triangleq [\mathbf{P}_1, \cdots, \mathbf{P}_K]$, the precoding optimization problem for $\mathbf{P}$ is given as

$$\begin{aligned}&\arg\max_{\mathbf{P}} \sum_{k=1}^{K}\mathrm{SE}_k, \\ &\text{s.t.} \quad \left|[\mathbf{P}_\mathbf{k}]_i\right|^2 = 1, \text{for } i = 1, ..., N_V.\end{aligned} \tag{14}$$

In order to simply the problem, all the antennas are assumed to utilize the full available power. The constant modulus constraint of the phase shifter for precoders is denoted as $\left|[\mathbf{P}_\mathbf{k}]_i\right|^2 = 1, \text{for } i = 1, ..., N_V$, and $[\mathbf{P}_\mathbf{k}]_i$ represents the i-th element of $\mathbf{P}_\mathbf{k}$. It is demonstrated that the problem is non-convex with the precoding variables.

III. Precoding Design Neural Network

Considering the high complexity of traditional optimization-based methods for the non-convex problem, in this section we propose a DL-based complex value neural network architecture that directly outputs $\mathbf{P}$ to solve (14).

A. PDNN Architecture

As illustrated in Table 1, our network consists of a flatten layer after the input layer, four dense layers with four activation functions. In order to stablize the training process and enhance the convergence, the batch normalization (BN) layers are utilized before each dense layer. There are 1024, 512, 256 and KN_V neurons for each dense layer, respectively. The first three dense layers take ReLu activation function and the last dense layer utilizes Sigmoid. There is no activation function or trainable parameters in the input, flatten and the self-defined Lambda layer, which is employed to implement specific functionality. Different from previous works [15]–[17] that divide the input into separated real and imaginary parts, PDNN is a complex valued neural network with plural inputs and outputs, which has been validated to exhibit superior performance in complex wireless signal processing.

TABLE I: The architecture of proposed PDNN.

Layer Name	Parameters Dim.	Activation Func.
Input Layer	$K \times N_V \times N_B \times L$	/
Flatten Layer	$(K \times N_V \times N_B \times L) \times 1$	/
Dense Layer 1	1024×1	ReLu
Dense Layer 2	512×1	ReLu
Dense Layer 3	256×1	ReLu
Dense Layer 4	$(K \times N_V) \times 1$	sigmoid
Lambda Layer	$K \times N_V$	/

1) Input and output: Given the presence of inter-UE interference in MU-MIMO scenario, it is imperative to collectively account for the one-to-one channels between all MRs and UBSs in a comprehensive manner. Therefore, the $K \times N_V \times N_B \times L$ four-dimensional complex matrix is fed into PDNN and then transformed into a one-dimensional complex vector accordance with its elements sequence in the flatten layer.

Inspired by [15], a Lambda layer, which does not contain any trainable parameters, is utilized for constant modulus constrained output of PDNN. The dimensional size remains unchanged after the output of Lambda layer. This layer converts the parameters of the previous layer's output α into the arrangement of all precoding vectors $\mathbf{P}$ as the following equation

$$\mathbf{P}_k = \exp(j \cdot 2\pi\alpha_\mathbf{k}) = \cos(2\pi\alpha_\mathbf{k}) + j \cdot \sin(2\pi\alpha_\mathbf{k}). \tag{15}$$

2) Unsupervised learning and loss function: Different from traditional supervised learning that requires labels for dataset,

the proposed PDNN employs an unsupervised learning method by leveraging a custom-defined loss function as following, which is directly related to problem (14),

$$\text{Loss} = -\frac{1}{\text{N}} \sum_{\text{n}=1}^{N} \sum_{k=1}^{K} \text{SE}_k, \tag{16}$$

where N representing the total number of dataset samples. The descent of loss function corresponds to an improvement of average total SE. And the convergence of loss function implies the approximation of optimal value for $\mathbf{P}$.

B. Training and Predicting

The application of PDNN involves two stages: training and predicting. In the training stage, position samples of certain train track segments are taken randomly and the LoS component is calculated by (4). Next all the LoS channels between each MR and each UBS are fed into PDNN. Then the PDNN generates the optimized $\mathbf{P}$ by minimizing the self-defined loss function with the historical channel data at corresponding locations. Through this approach, it is feasible for PNDD to learn the precoding design scheme for all the MRs within specific railway section with strong LoS component and be robust to the randomness of locations.

In the predicting stage, the well-trained PDNN is utilized to implement feedback-free precoding design. The LoS estimation mapped from practical position of HST is fed into PDNN to obtain optimized precoding for each MR. With fixed parameters, PDNN will output the optimal joint precoding corresponds to the solution for (16). To this end, the feedback-free mapping from location to joint precoding is accomplished.

IV. Simulation Results

We consider a simulation setup where L UBSs are uniformly and independently distributed along the 800 m railway track, and K MRs are uniformly distributed on the 200 m HST. Carrier frequency is $f = 2$ GHz and all MRs utilize full transmission power. The noise power is $\sigma^2 =$ -4 dBm and the Rician factor R = 20 dB. We use average $\text{SE} = \sum_1^K \text{SE}_k/K$ to evaluate performance. The feedback latency of channel information exhibits a random distribution within the range of 50-100ms, based on the current GSM-R standard [18]. Despite the delay, it is assumed that the conventional feedback-based approach can acquire accurate channel information from the pilot. Due to the feedback latency and high speed, the channel obtained through feedback at a given position, such as 100 meters, is considered to be an accurate representation of the channel at an early location, e.g., $(100 - v * t_{feedback})$ meters. Moreover, the feedback accuracy deteriorates as the velocity increases.

During the training process, we make a variation comparison between train and validation loss as shown in Fig. 2. It shows that the train and validation loss converges to approximately the same minimum value within 30 epochs, which indicates that the computational resource PDNN requires is minimal in the training process.

Fig. 3(a) compares the SE at different positions of HST at a speed of 350 km/h in the cellular, small cell and FD-RAN systems, respectively. The deployment of BSs in small cell system is the same with FD-RAN, while the cellular system consists of one cellular BS with same total number of antennas. PDNN is utilized for all the architectures. We can see that the small cell returns the worse performance than FD-RAN architecture because the large inter MR interference can not be eliminated by independent signal detection. Moreover, HST communications with cellular system is also considered for comparison and higher SE can be achieved when HST is close to the cellular BS. However, it exhibits poor SE at the position of cell edge. From cumulative probability function (CDF) of these transmission schemes shown in Fig. 3(b), we observe that the difference between maximum and minimum SE value for cellular system is significantly greater than the other two architectures. Therefore, compared with small cell and cellular systems, the FD-RAN architecture can provide both higher and more steady SE performance in HST communications.

The average SE against various speed of HST in FD-RAN system with different precoding design scheme is shown in Fig. 4. It is shown that the average SE of feedback-free FD-RAN is similar with respect to different HST speeds. On the contrary, although zero-forcing (ZF) precoding demonstrates superior performance at lower velocities, its performance drops below feedback-free transmission as the speed reaches 300km/h. At such high speeds, the latency of feedback will lead to inaccurate channel information, affecting the perfor-

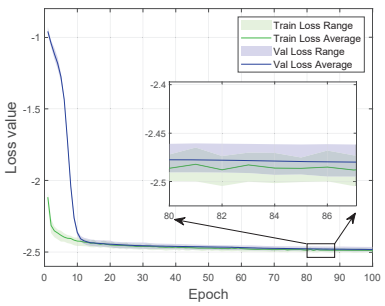

Fig. 2: Loss curve during training process.

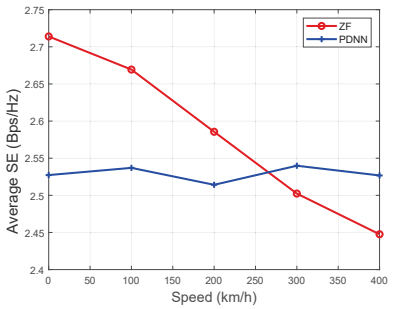

Fig. 4: SE v.s. speed with different precoding schemes.

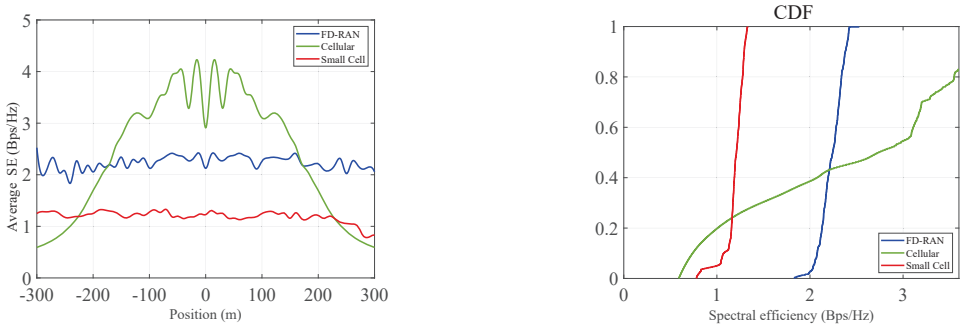

(a) (b)

Fig. 3: (a) SE against the position of HST in FD-RAN, small cell and cellular systems. (b) CDF of per-position SE for HST in different system (N_B = 4, L = 9, N_V = 2, K = 8, v = 350km/h, R = 20dB, $N_B^{cellular} = N_B L$, d^{ve}= 30m).

mance of ZF precoding. Note that the analysis presented here solely focuses on the performance degradation resulting from the latency in feedback-based transmission schemes. Considering the pilot and feedback overhead saved in feedback-free approaches, the SE gap would be further widened.

V. Conclusion

In this paper, we have proposed a location-based precoding design method without channel information feedback in a linear structured HST communications system under the FD-RAN architecture. Additionally, a neural network have been exploited to implement the location-precoding mapping in an unsupervised way with our designed loss function based on uplink SE. Simulations have demonstrated that the method could achieve better performance against traditional ZF precoding scheme in high mobility communications. Moreover, compared with small cell or current cellular architectures, FD-RAN can offer improved and stable SE at all positions. In future work, we are going to investigate the orthogonal frequency division multiplexing (OFDM) technology for MU-MIMO HST communications and verify the influence of various Rician factor on the HST communication performance.

References

[1] B. Ai, A. F. Molisch, M. Rupp, and Z.-D. Zhong, "5G key technologies for smart railways," *Proceedings of the IEEE*, vol. 108, no. 6, pp. 856–893, 2020.

[2] J. Zheng, J. Zhang, L. Zhang, X. Zhang, and B. Ai, "Efficient receiver design for uplink cell-free massive MIMO with hardware impairments," *IEEE Transactions on Vehicular Technology*, vol. 69, no. 4, pp. 4537–4541, 2020.

[3] T. Li, Z. Chen, P. Fan, and K. B. Letaief, "Position-based power allocation for uplink HSRs wireless communication when two trains encounter," in *2016 IEEE Global Communications Conference (GLOBECOM)*. IEEE, 2016, pp. 1–6.

[4] D. He, B. Ai, K. Guan, Z. Zhong, B. Hui, J. Kim, H. Chung, and I. Kim, "Channel measurement, simulation, and analysis for high-speed railway communications in 5G millimeter-wave band," *IEEE Transactions on Intelligent Transportation Systems*, vol. 19, no. 10, pp. 3144–3158, 2017.

[5] Q. Yu, H. Zhou, J. Chen, Y. Li, J. Jing, J. J. Zhao, B. Qian, and J. Wang, "A fully-decoupled RAN architecture for 6G inspired by neurotransmission," *Journal of Communications and Information Networks*, vol. 4, no. 4, pp. 15–23, 2019.

[6] Z. Liu, K. Yu, T. Zhang, J. Liu, J. Chen, H. Zhou, and X. S. Shen, "Leveraging deep reinforcement learning for geolocation-based MIMO transmission in FD-RAN," in *2023 IEEE/CIC International Conference on Communications in China (ICCC)*, 2023, pp. 1–6.

[7] Z. Yang, L. Chen, and W. Wang, "Location and attitude information aided codeword selection in millimeter wave MIMO system," in *2022 2nd IEEE International Symposium on Joint Communications and Sensing (JCS)*, 2022, pp. 1–6.

[8] J. Zheng, J. Zhang, E. Björnson, and B. Ai, "Impact of channel aging on cell-free massive MIMO over spatially correlated channels," *IEEE Transactions on Wireless Communications*, vol. 20, no. 10, pp. 6451–6466, 2021.

[9] J. Zheng, J. Zhang, E. Björnson, Z. Li, and B. Ai, "Cell-free massive MIMO-OFDM for high-speed train communications," *IEEE Journal on Selected Areas in Communications*, vol. 40, no. 10, pp. 2823–2839, 2022.

[10] L. Liu, C. Tao, J. Qiu, H. Chen, L. Yu, W. Dong, and Y. Yuan, "Position-based modeling for wireless channel on high-speed railway under a viaduct at 2.35 GHz," *IEEE Journal on Selected Areas in Communications*, vol. 30, no. 4, pp. 834–845, 2012.

[11] K. Xiong, B. Wang, C. Jiang, and K. R. Liu, "A broad beamforming approach for high-mobility communications," *IEEE Transactions on Vehicular Technology*, vol. 66, no. 11, pp. 10 546–10 550, 2017.

[12] J. Zhao, Q. Yu, B. Qian, K. Yu, Y. Xu, H. Zhou, and X. Shen, "Fully-Decoupled Radio Access Networks: A Resilient Uplink Base Stations Cooperative Reception Framework," *IEEE Transactions on Wireless Communications*, 2023.

[13] A. Hjorungnes and C.-V. M. Derivatives, "With applications in signal processing and communications," *Cambridge Univ Pr*, 2011.

[14] Z. Wang, J. Zhang, B. Ai, C. Yuen, and M. Debbah, "Uplink performance of cell-free massive MIMO with multi-antenna users over jointly-correlated rayleigh fading channels," *IEEE Transactions on Wireless Communications*, vol. 21, no. 9, pp. 7391–7406, 2022.

[15] T. Lin and Y. Zhu, "Beamforming design for large-scale antenna arrays using deep learning," *IEEE Wireless Communications Letters*, vol. 9, no. 1, pp. 103–107, 2019.

[16] P. Zhang, L. Pan, T. Laohapensaeng, and M. Chongcheawchamnan, "Hybrid beamforming based on an unsupervised deep learning network for downlink channels with imperfect csi," *IEEE Wireless Communications Letters*, vol. 11, no. 7, pp. 1543–1547, 2022.

[17] J. Xue, K. Yu, T. Zhang, H. Zhou, L. Zhao, and X. Shen, "Cooperative deep reinforcement learning enabled power allocation for packet duplication urllc in multi-connectivity vehicular networks," *IEEE Transactions on Mobile Computing*, 2024.

[18] R. He, B. Ai, G. Wang, K. Guan, Z. Zhong, A. F. Molisch, C. Briso-Rodriguez, and C. P. Oestges, "High-speed railway communications: From GSM-R to LTE-R," *IEEE VehIcular Technology MagazIne*, vol. 11, no. 3, pp. 49–58, 2016.